

Spatiotemporal Pinpoint Cooling Sensation Produced by Ultrasound-Driven Mist Vaporization on Skin

Mitsuru Nakajima¹, Member, IEEE, Keisuke Hasegawa², Member, IEEE, Yasutoshi Makino¹, and Hiroyuki Shinoda², Member, IEEE

Abstract—In this study, we achieved a noncontact tactile display that presents a pinpoint and instantaneous cooling sensation on the skin surface with no devices directly in contact with the user's body. We employed ultrasound phased arrays to generate a focused ultrasound, which locally and instantaneously expedites the vaporization of room-temperature water mist floating near the surface of the user's skin, offering a sudden pinpoint cooling sensation. In this article, we describe the physical configuration of the proposed method and show the measurement results, demonstrating how the user's skin surface was cooled. During the experiments, we discovered that a part of the skin exposed to a focused ultrasound within the floating mist was selectively cooled with negligible delay. Our prototype system offers a cooling spot of approximately 15 mm in diameter, which causes a temperature decrease of 4.6 K in 1 s and 3.3 K in the first 0.5 s on a hand situated 500 mm away from the device. Additionally, the ultrasound-driven cooling spot can be controlled on the skin surface, which is felt as a cool moving spot. Such a position-free cooling system with a high spatiotemporal resolution will open the door to unprecedented practical tactile applications.

Index Terms—Cooling sensation, focused ultrasound, mist vaporization, non-contact thermal display.

I. INTRODUCTION

MIDAIR haptics originating from [1] [2] and growing in this decade [3] [4] has been mainly focused on vibrotactile sensation provided by ultrasonic radiation pressure [5]. This is because the force on the skin is one of the primary parameters governing the tactile sensation. However, we also know that mechanical stimuli alone cannot cover all tactile experiences. Thermal sensation is also a crucial component of both tactile sensation as well as pain sensation [6] [7] [8]. The thermal conductivity sensed by the thermal receptors provides a clue for

material identification [9] [10], as well as the perception of temperature in the environment such as “hot” and “cold” [11]. It is expected that remotely displaying these senses will offer more realistic and enriched haptic experiences.

The majority of application-oriented research on thermal displays is based on heat conduction using a wearable device with Peltier elements [12]– [16]. There is also a method in which water is applied as the heat medium [17] [18], where multiple flow channels are selectively actuated to convey hot and cold water to offer prompt temperature changes. Another method has been shown in which thermal sensation is displayed by controlling the humidity of the air around a body [19].

A few studies have been conducted on non-contact and remote thermal displays to stimulate local parts of the skin in the workspace with no device worn. For a remote heating display, radiation-based localized and prompt heating methods using a laser and infrared rays have been proposed [20]– [24]. These methods can control the irradiation position by using optical systems composed of lenses and Galvano mirrors. On the other hand, similar practical methods have not been established for arousing a remote cooling sensation. The most straightforward method is the midair transport of cold air with a fan, blower, or vortex tube, where it is difficult to display a cooling sensation locally and instantaneously over a long distance [25].

We addressed the realization of a remote cooling sensation display using a focused ultrasound emitted by airborne ultrasound phased arrays, which accompanies localized nonlinear acoustic phenomena. As a first attempt, we proposed transporting cooled air to the skin surface in mid-air using an ultrasound beam generated by ultrasound phased arrays [26], which caused an ultrasound-driven airflow, which is technically called acoustic streaming [27]. Similarly, we proposed a method in which a water mist is transported in air based on the same principle, and the skin surface is cooled by the vaporization of the mist [28] [29]. We found that this heat-of-evaporation-based technique is advantageous in that the mist can be at room temperature, unlike the initial air-transportation-based method requiring pre-cooled air storage.

In this paper, we propose a more sophisticated version of a remote cooling sensation display, where a focused ultrasound expedited vaporization of the water mist around the skin to display in a quite pinpoint and instantaneous fashion. As a result, prompt cooling sensation confined in a spot as large as a fingertip can be aroused, which cannot be achieved by the previous method that merely create ultrasound-driven airborne path of

Manuscript received October 15, 2020; revised April 3, 2021; accepted May 30, 2021. Date of publication June 4, 2021; date of current version December 16, 2021. This work was supported by the JSPS KAKENHI under Grant 16H06303 and JST CREST JPMJCR18A2. This article was recommended for publication by Associate Editor Kyle Brandon Reed and Editor-in-Chief Domenico Prattichizzo upon evaluation of the reviewers' comments. (Corresponding author: Mitsuru Nakajima.)

Mitsuru Nakajima, Yasutoshi Makino, and Hiroyuki Shinoda are with the Department of Complexity Science and Engineering, The University of Tokyo, Chiba 277-8561, Japan (e-mail: nakajima@hapis.k.u-tokyo.ac.jp; yasutoshi_makino@k.u-tokyo.ac.jp; hiroyuki_shinoda@k.u-tokyo.ac.jp).

Keisuke Hasegawa is with the Department of Information Physics and Computing, The University of Tokyo, Tokyo 113-8656, Japan (e-mail: keisuke_hasegawa@ipc.i.u-tokyo.ac.jp).

Digital Object Identifier 10.1109/TOH.2021.3086516

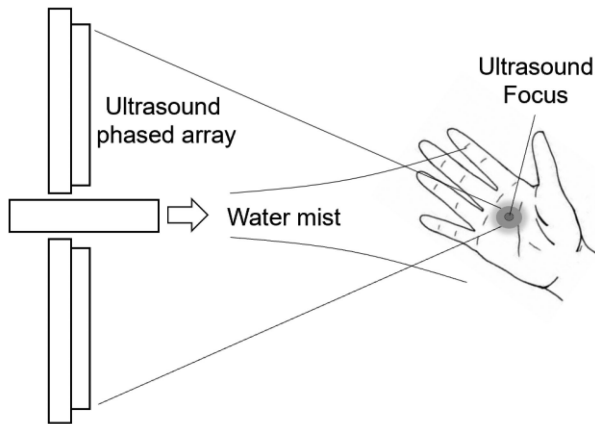


Fig. 1. Overview of the proposed method. The mist converged by focused ultrasound can be rapidly vaporized and display a cooling sensation.

water mist [29]. In our newly proposed method, a focused-ultrasound irradiation in a mist-filled workspace produces a cool spot without a long-distance mist transportation (Fig. 1).

A water mist at room temperature is easy to generate, and an ultrasound focus can be generated at an arbitrary three-dimensional position in front of the phased array. Therefore, the mist-ultrasound combination has the potential to produce various effects in practical scenes. A transparent aerial display has already been reported by forming and controlling mist in the form of aerosol using an acoustic beam generated from ultrasound phased array [30]. Furthermore, a study [31] reported mist-flow control by sound fields in non-contact tactile feedback and object manipulation.

In the following sections, we measure the spatiotemporal properties of the cooling method and clarify the conditions for effective cooling. We also demonstrate that the motion of a cooled spot is displayed when the focused ultrasound moves on the skin surface.

II. PROPOSED METHOD

A. System Overview

The overall schematic of the proposed system is shown in Fig. 2. It is composed of 40 kHz ultrasound phased arrays, a duct for emitting mist, and a water tank (20 L) for mist storage. A duct hose is located at the center of the phased arrays such that it faces the same direction as the phased array surface. An ultrasonic atomizer for generating mist, the resonant frequency of which is approximately 1.6 MHz (IM6-36D/S SEIKO GIKEN, Inc.), is contained in the tank. At the highest power, the atomizer can produce 4000 ml of water mist per hour. The particle diameter of the generated mist which was measured by a manufacturing company was 4~5 μm . The tank was connected to a DC fan (San Ace 60W SANYO DENKI Co.) and a duct hose.

B. Generation of Ultrasonic Focus Using Ultrasound Phased Array System

We use an airborne ultrasound tactile display system [32] [33] based on the same principle as in [1]– [4]. 249 transducers (T4010A1, Nippon Ceramic Co., Ltd.) are arranged in

a planar lattice on this device, which composes ultrasound emitting aperture with the size of 182.9 mm \times 142.6 mm. By integrating 4 devices as shown in Fig. 2(a), the aperture of phased array can be enlarged. This device can create a sound field with various spatial distributions by controlling the phase delays and amplitudes of the output waveform of each transducer. Based on this principle, we create a focused ultrasound at an arbitrary desired position on the skin exposed to a mist. The focusing method is the same as in [1]– [4] [32] [33]. The phase of the output ultrasound from each transducer was determined to compensate for the phase delay proportional to the distance between each transducer and the focus. We used a single focus in all the following experiments in this paper.

C. Remote Displaying Cooling Sensation

When the fan is operating, the air is blown into the inside of the tank and mist is discharged from the duct. The fan is connected to the stabilized power source, and the amount of mist emission can be controlled by adjusting the driving voltage of the fan. A portion of the mist discharged from the duct is transported in the air and drifts near the surface of the user's skin. Based on the subjective perceptions of the authors, no cooling sensations were aroused when merely touching the floating mist in air. However, we could clearly perceive our skin surface being cooled when focused ultrasonic irradiation was superimposed on the skin. We evaluate and clarify this phenomenon in the following sections.

III. EXPERIMENT 1

A. Experiment Outline

Using the system described in Section II, we conducted a comparative experiment on the cooling effect under the following three conditions: irradiation of i) focused ultrasound on a skin, ii) exposure of the skin to a mist, and iii) simultaneous combination of i) and ii). More specifically, the aim of this experiment is to assess how the cooling effect under the condition iii) is enhanced in comparison with the other conditions. For each case, the measurement was conducted three times. The palm used in the experiment was that of one of the authors (male, 27 years old). This palm was also used in Experiments 2 and 3. For the experimental environment, the temperature of the room and the level of humidity were 25°C and 60 %, respectively. Experiment 2 was also conducted under the same conditions. Each time before measuring the surface temperature of the palm, we placed the palm on a hot plate (NHP-M30N) set to 309 K (36°C) for 60 s.

B. Measurement Procedures and Experimental Result

For each of the three cases, as shown in Fig. 3(i), we placed our hand 50 cm away from the ultrasound phased array surface. At this time, we adjusted the position of the center of the palm such that the plane of the user's palm and the phased array were parallel to each other.

We evaluated the cooling effect of the three cases based on the temporal temperature changes on the skin surface after ultrasound

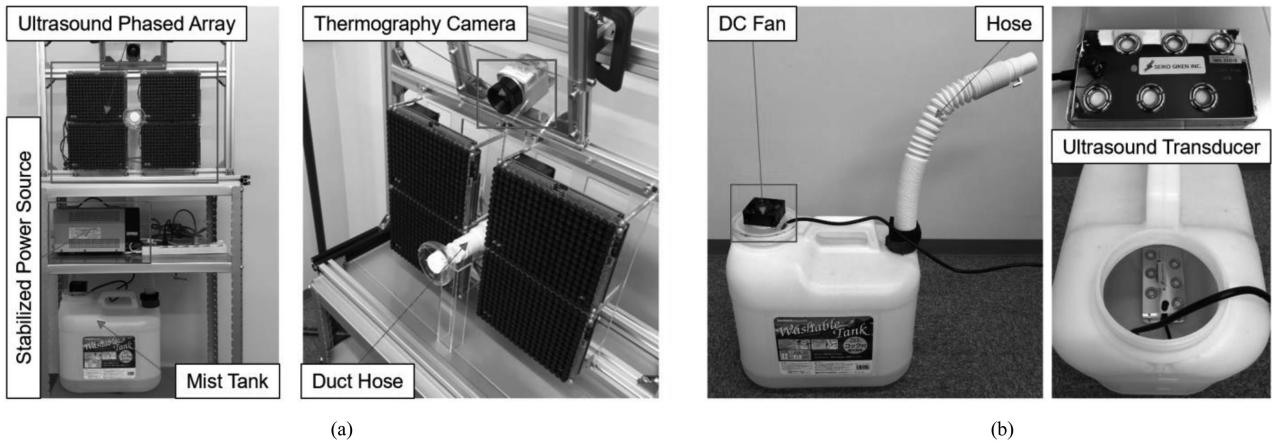


Fig. 2. Prototype display. The overall system is composed of ultrasound phased array and mist generator. The mist generator is composed of an ultrasound transducer in the tank, hose, and DC fan connected to a stabilized power source. (a) Overall view (b) Mist generator.

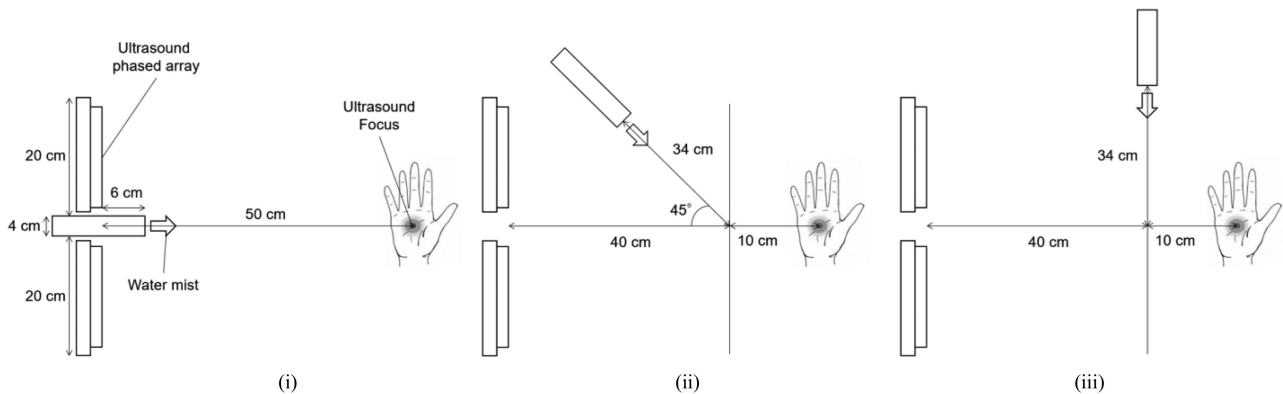


Fig. 3. Experimental setup and view from above.

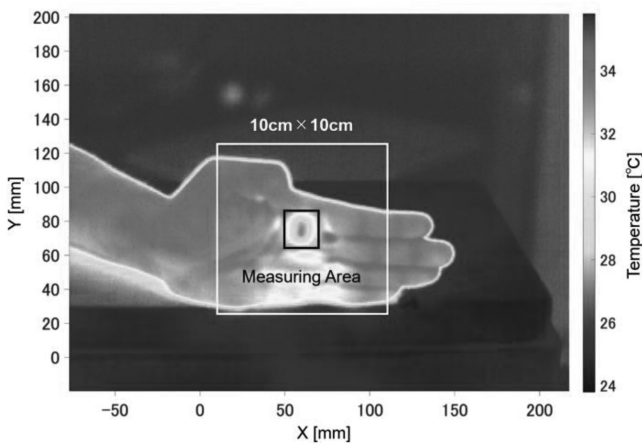


Fig. 4. Target parts on measurement area in the thermographic image.

irradiation. We captured the entire palm using a system with a thermographic camera (PI450, Optris) in video format. This thermographic camera does not need manual calibration in standard use. We determined the measurement area ($50 \text{ mm} \leq X \leq 65 \text{ mm}$, $64 \text{ mm} \leq Y \leq 88 \text{ mm}$), as shown in Fig. 4.

Fig. 5 shows the temperature changes for the three cases. Each plot shows the minimum value of the temperature within

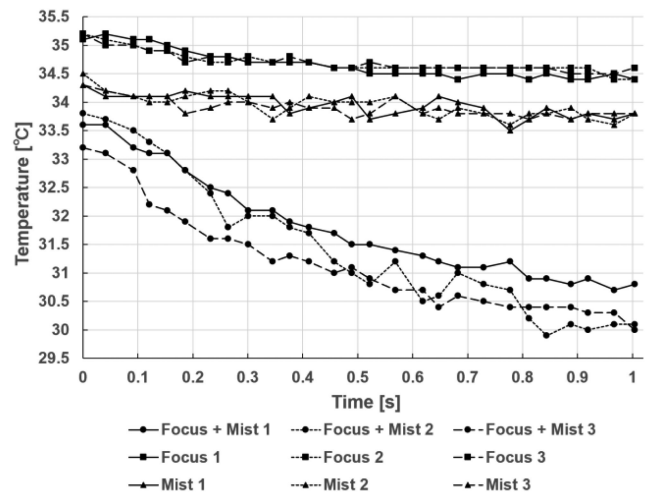


Fig. 5. Temperature change when using focused ultrasound, mist, or both.

the measurement area at each time. Under the Mist condition, the time origin was defined as the moment when the air blowing fan was turned on and the mist is sent out into the room. Under the Focus condition, the origin is the moment when the ultrasound is turned on. When the speed of sound is assumed to be 340 m/s , the time required to propagate over a distance of 50 cm

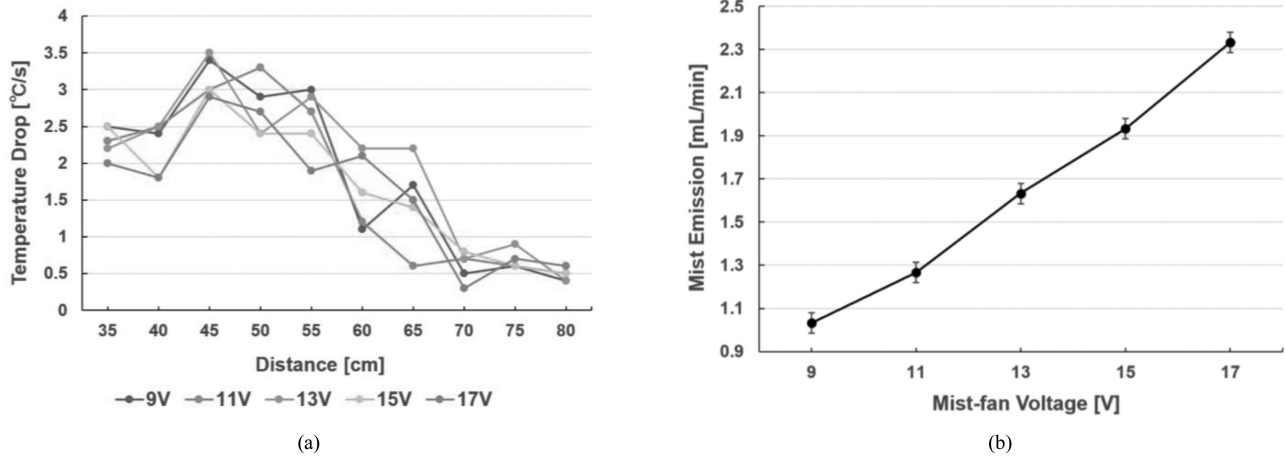


Fig. 6. (a) Temperature drops versus the distance from the ultrasound device and (b) quantitative relationship between the mist-fan voltage and amount of mist emission.

is approximately 1.5 ms, which is sufficiently short compared to the sampling interval. Under the Focus+Mist condition, the origin is the moment when the ultrasound is turned on while the space is filled with mist. It was found that the temperature rapidly decreased when the focused ultrasound was displayed on the skin surface exposed to the mist. In this case, we observed a surface temperature drop of 2.1 to 2.9 K in 0.5 s and 2.8 to 3.7 K in 1 s, with the variation between trials less than 1 K. This result indicated that the palm surface was physically cooled by ultrasound irradiation of the water mist. It is considered that the vaporization of small mist is more active in Focus+Mist condition than the other cases.

IV. EXPERIMENT 2

A. Experiment Outline

Using a system similar to Experiment 1, we obtained the relationship among the temperature drops on the skin surface, the amount of water mist ejected, and the distance from the phased array surface. The purpose of this experiment was to clarify the valid spatial range of the proposed system and the required density of the mist. The amount of mist emitted was controlled by the applied voltage to the fan supplied using a stabilized power source. We measured the temperature drops versus palm position from the device by varying the mist-fan voltages.

We also connected another measurement of the temperature changes in the cases of (i), (ii), and (iii) in Fig. 3 to evaluate the effect of the discharge direction of the mist under a constant flow of mist.

B. Measurement Procedures

In each measurement, we first placed the palm on a hot plate (NHP-M30N) set to 309 K (36°C) for 60 s. After this initialization process, we measured the surface temperature distribution of the palm using a thermographic camera, whereas the cooling sensation was displayed using a focused ultrasound as applied in Experiment 1.

First, we investigated five cases in which the distances between the palm and ultrasound device were 35, 40, 45, 50, 55, 60, 65, 70, 75, and 80 cm. We evaluated the temperature drop by changing the mist-fan voltage across 9, 11, 13, 15, and 17V. In this experiment, we define the temperature drop as the temperature change from the initial time of the cooling process to 1 s later.

Next, the measurement was performed under Mist+Focus condition by changing the direction of mist supply in the three directions shown in Fig. 3. The position of the focus was 50 cm from the phased array surface. The mist-fan voltage was 13 V.

The measurement was conducted three times in the same manner as in Experiment 1. Similar to Experiment 1, there was little variation in the data across each trial. Therefore, we show a representative result for each experiment in the following part of the paper.

C. Experimental Results and Discussion

Fig. 6(a) shows the temperature drops at each mist-fan voltage against the distance from the ultrasound device. The relation between mist-emission amounts and mist-fan voltages is shown in Fig. 6(b). For distances between 35 and 50 cm, the difference in temperature drop was less than 1 K regardless of the mist-fan voltage conditions. By contrast, for distances between 55 and 65 cm, a larger variance was observed. At distances of greater than 70 cm, the temperature drop was less than 1 K. Based on the results of the temperature drop, the feasible distance was found to be 45 to 50 cm. Up to that distance, the performance of the cooling effect was stable regardless of the mist generation as far as the tested voltage was concerned.

Fig. 7 shows the temperature change with respect to the direction of the mist emitted. The temperature change increases in order of cases (i), (ii), and (iii).

The results shown in Fig. 6 indicate that the proposed system requires a certain amount of water mist around the palm, although the effect is saturated against the density of the mist. Under the experimental conditions, the main factor

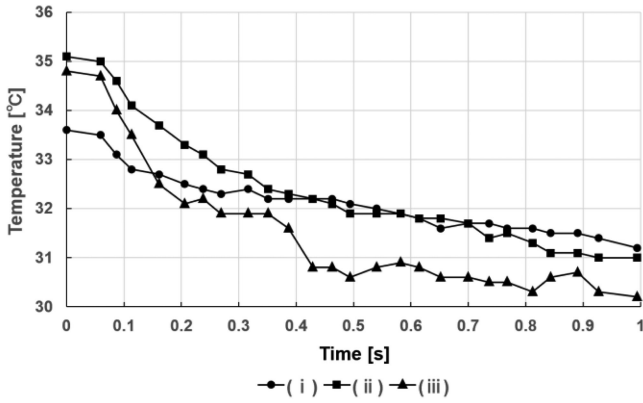


Fig. 7. Temperature change when the direction of mist emission was changed as shown in Fig. 3(i), (ii), and (iii).

determining the cooling effect is the ultrasound power density around the palm, which decreases beyond 50 cm.

At the same time, Fig. 7 suggests that the direction of the mist influences the cooling effect. The variable factors among the three cases are the liquid-water density and vapor pressure near the skin surface. In case (i), the mist is already evaporated in the ultrasound beam, while in case (iii), a fresh mist is supplied to the skin surface and vaped water is removed by the stream along the skin. This is the possible reason why case (iii) shows the largest temperature drop among the three cases.

V. EXPERIMENT 3

A. Experiment Outline

During this experiment, we measured the spatiotemporal temperature distribution on the palm for a long duration using a thermographic camera. First, we measured temporal temperature changes in the spot region and obtained horizontal temperature distributions with a cross-sectional axis passing through the spot center. We also conducted a measurement in which the cold spot traveled on the palm. This experiment was conducted under a room temperature and humidity of 24°C and 55 %, respectively.

B. Measurement Procedures

We set the position of the focused ultrasound at 50 cm distant from the surface of the phased array, as in Experiment 1. In addition, similar to the former experiments, we placed the palm such that the focused ultrasound hit the center of the palm as shown in Fig. 3(i). We then captured the video image of the palm while it was cooled by the mist vaporization.

The measuring time was 20 s. We started irradiation with a focused ultrasound at 5 s after the measurement began. Irradiation continued for 10 s and ceased during the last 5 s. We defined the measurement area hereafter as a rectangular region containing the cooling spot, as shown in Fig. 4. Fig. 8 shows the measuring axis ($Y = 73$ mm), which represents a specified position for the cross-sectional measurement of the temperature distribution on the palm.

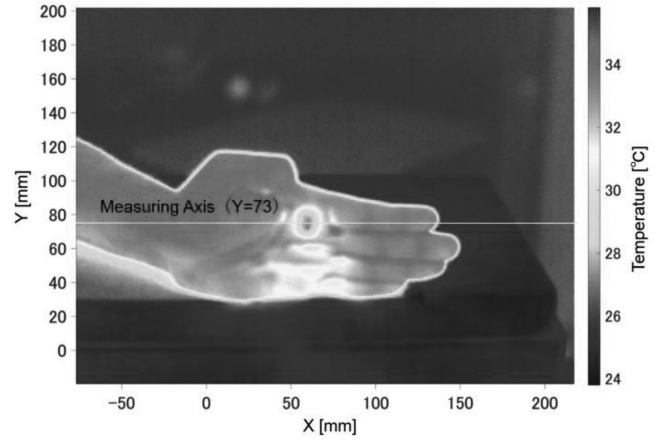


Fig. 8. Target parts on measuring axis in the thermographic image.

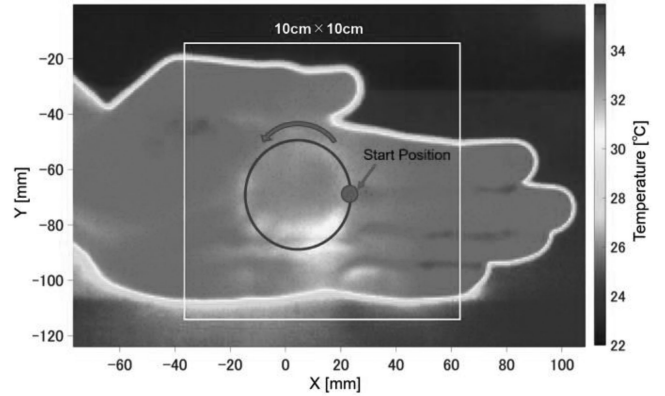


Fig. 9. Start point of the cold spot, circular trajectory and motion direction are shown in the thermographic image.

Next, the focused ultrasound repetitively traveled in a counterclockwise direction with a radius of 2 cm under a rotation period of 5 s. The start position, rotational position, and rotational direction are shown in Fig. 9. We shot a video in which the ultrasound focus traveled during a single period.

C. Experimental Results

Fig. 10 shows the long-term temperature change for a still cooling spot. Fig. 11 shows the minimum value of temperature versus time in the measuring area. In these figures, we define the time origin ($t = 0$) as the start of the measurement. It means that the focused ultrasound is irradiated at $t = 5$ s and stopped at $t = 15$ s. It is clearly indicated that the irradiation of the focused ultrasound yielded a cold spot causing a rapid temperature decrease in 1 s. Next, the temperature was continuously lowered while the focused ultrasound was being irradiated. After irradiation for 10 s, the temperature finally dropped by 7.8 K. After the ultrasound irradiation stopped, the temperature started to increase.

Fig. 12 shows the cross-sectional temperature distribution on the measuring axis shown in Fig. 8. The temporal changes in the temperature pattern are plotted for $t = 5$ to 15 s. The size of the cold spot was kept at approximately 2 cm, whereas a peripheral semi-cold area was gradually formed around the cold spot. Since

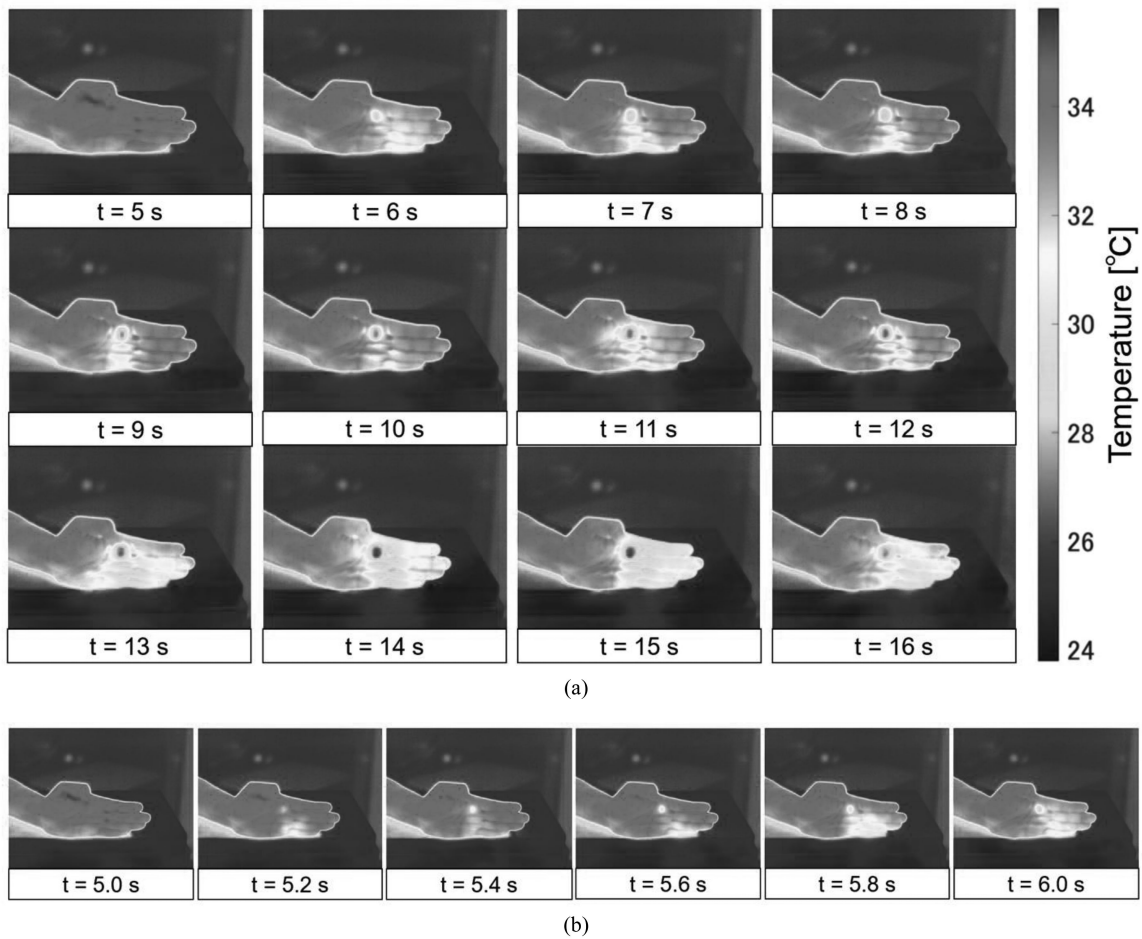


Fig. 10. Temporal change of skin cooled by converged mist. The focused ultrasound was generated at 5 s and stopped at 15 s. They show the temperature changes (a) 1 s and (b) 200 ms intervals from the start of irradiation.

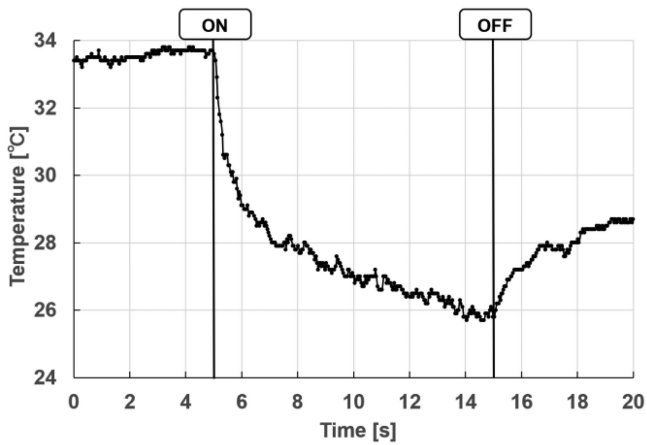


Fig. 11. Temperature change from the focused ultrasound.

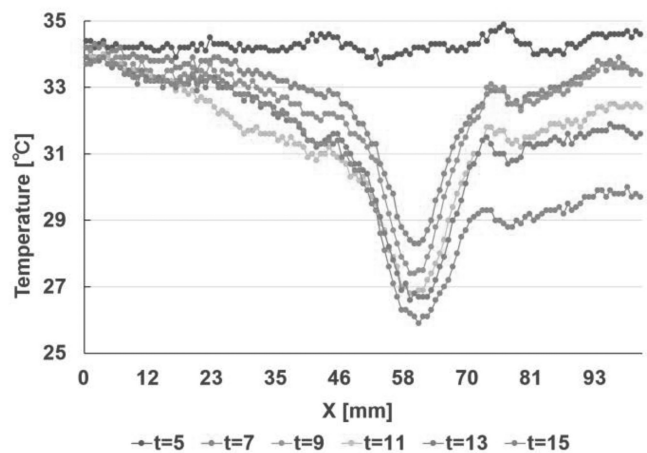


Fig. 12. Temperature distribution in measuring axis.

both the mist flow and the palm surface are not symmetric, the temperature distribution was asymmetric.

Fig. 13 shows sequential images when the cold spot moved for one period on the circular path. A circular trace on the palm is clearly observable, which indicates a continuous movement of a cooled spot on the palm. Subjectively, the authors perceived a clear spot and the exact position of the spot.

VI. VERIFICATION OF COOLING ABILITY

A. Measurement of Heat Flux

The cooling process proposed in this paper consists of two phases: acceleration of the water vaporization by ultrasound and cooling the inside of the skin by thermal conduction.

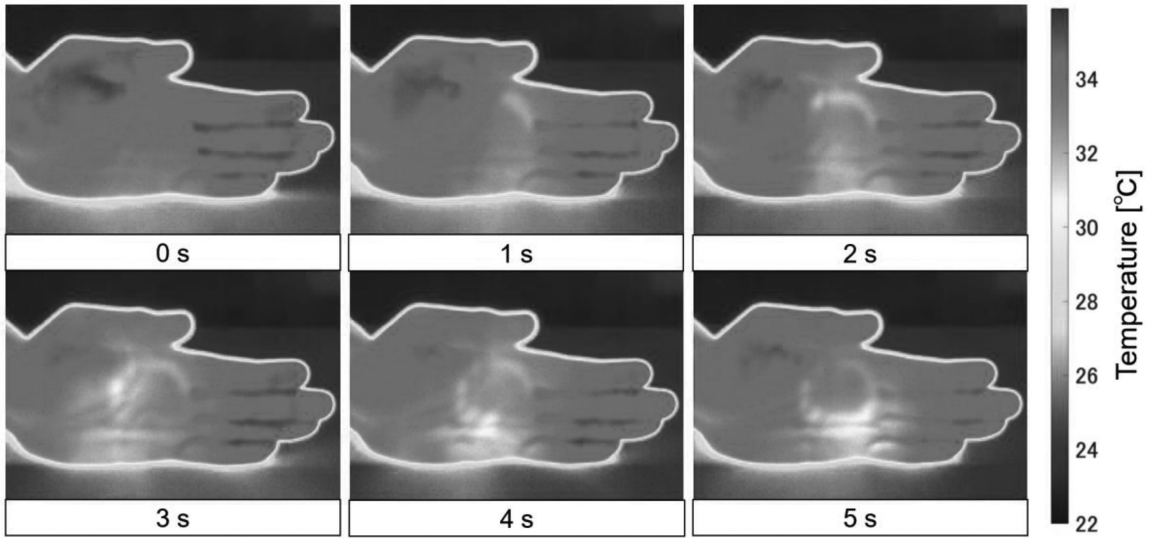


Fig. 13. Temporal change on the skin when a cold spot rotates one round. The movement of the cold spot started at 0 s. At 5 s, cold spot completed one lap.

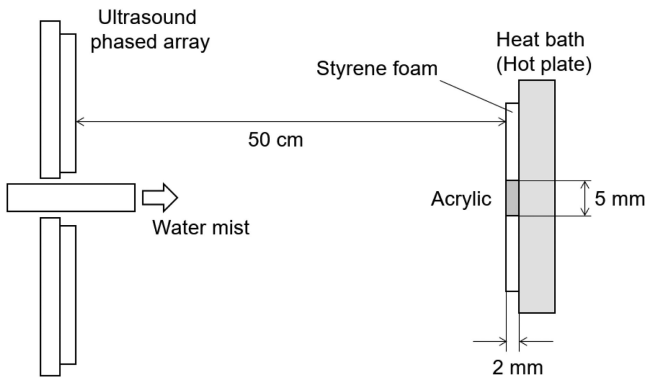


Fig. 14. Schematic of heat flux measurement.

The mechanism of the first phase to facilitate vaporization of the water on the skin or particles of the water mist is currently unclear in detail and is not addressed in this paper. However, since the heat capacity and thermal conductivity of air are significantly smaller than those of the skin, it is sure that vaporization by the converged ultrasound in the vicinity of the skin surface is the major factor while the thermal conduction in the air across a long distance is a minor factor.

Regarding the second phase, we will discuss the heat flux absorbed by the water vaporization as the fundamental parameter to evaluate the skin-cooling ability. We set up an experiment shown in Fig. 14 and 15 to simulate the skin cooling with a simplified model. As simulated skin, an acrylic plate is placed in contact with a heat bath of constant temperature T_2 at the backside, while the surface temperature T_1 is lowered by the water evaporation. When the surface temperature T_1 decreases and finally reaches a steady state, the heat flux q_s [W/m^2] at the surface to maintain the temperature difference $T_1 - T_2$ between the two ends satisfies

$$q_s = \frac{T_1 - T_2}{L_s / \lambda_s} \quad (1)$$

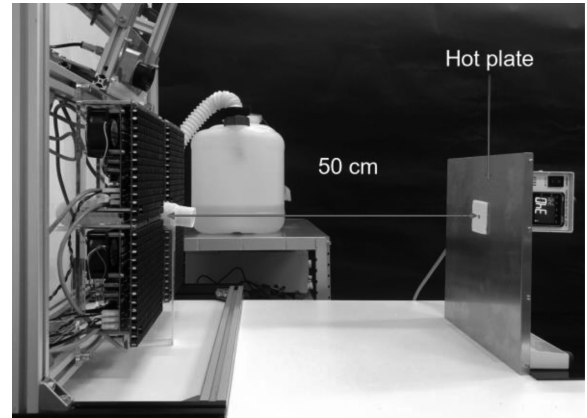


Fig. 15. Experimental setup. An acrylic block is surrounded by a styrene foam and greased at the boundary with the hot plate to bond them tightly.

where L_s [m] is the thickness, and λ_s [$\text{W}/(\text{m} \cdot \text{K})$] is the thermal conductivity of the acrylic plate. We obtain q_s by measuring T_1 using thermography.

As the object having a comparable thermal conductivity to the skin tissue, we used a square acrylic block whose side and thickness were 5 mm and 2 mm, respectively. The thermal conductivity of the acrylic is $0.21 \text{ W}/(\text{m} \cdot \text{K})$ in the literature. It was attached to the hot plate being surrounded by styrene foam to prevent heat transfer from the sides. Each object is cooled for 50 s, while the hot plate was set to be 34°C as the heat bath whose temperature was assumed to be constant during the experiment. Each measurement was conducted after heating the object for 5 minutes in advance.

Fig. 16 shows the temperature change during the cooling process. From the steady-state temperature estimated as 21.4°C , we evaluated the heat fluxes on the surface as $-1.3 \times 10^3 \text{ W}/\text{m}^2$ using Eq. (1) at the center of the ultrasound focus.

Note that when the actual skin is cooled, there are distributed heat sources inside the skin due to the blood flow. That is a factor to prevent the temperature drop inside the skin,

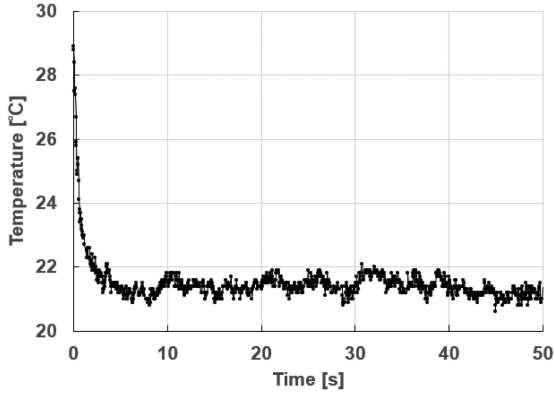


Fig. 16. Temperature change of the acrylic block surface.

therefore the final temperature for the “acrylic skin” shown in Fig. 16 is lower than the result of Fig. 11. However, we excluded this effect in the above theoretical analysis.

B. Comparison with Touch to Solid Object

Next, we compare the created temperature change to that of an actual contact to a solid object. It is known that a finger can identify the object’s material by the temperature drop at the moment of touch. In the paper [34], a precise model of contacting objects with different temperature is discussed, however, this paper uses a following simple model. Since we are interested in the short-term change around the contact moment, we consider the skin and object are both semi-infinite. Assuming that the skin temperature is T_S [K] and the temperature of the contacting object is T_M [K], the temperature T_C [K] at the contact boundary is given as

$$T_C = \frac{T_S - T_M}{1 + \mu_M/\mu_S} + T_M \quad (2)$$

after the contact where μ is thermal effusivity defined as

$$\mu = \sqrt{\rho c \lambda} \quad (3)$$

using density ρ [g/m³], specific heat capacity c [J/(g · K)], and thermal conductivity λ [W/(m · K)]. The subscript S and M denote the skin and the object.

Consider the temperature change inside the skin, letting the distance from the skin surface be x . The temperature change at position x inside the skin is given by the following equation by solving the diffusion equation:

$$T(t, x) = T_C + (T_S - T_C) \operatorname{erf}\left(\frac{x}{2\sqrt{\alpha_S t}}\right) \quad (4)$$

$$\alpha_S = \frac{\lambda_S}{c_S \rho_S} \quad (5)$$

$$\operatorname{erf}(x) = \frac{2}{\sqrt{\pi}} \int_0^x \exp(-t^2) dt \quad (6)$$

Fig. 17 shows the comparison between the theoretical values in the touch to various objects and the result of Fig. 11.

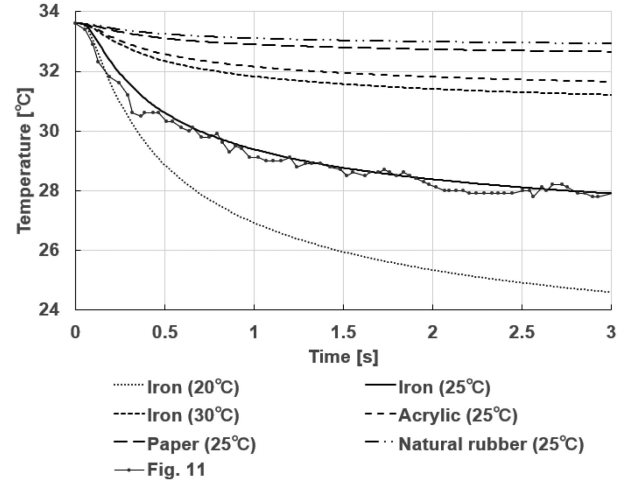


Fig. 17. The theoretical skin-temperature change at 0.3 mm from the skin surface when the skin touches various objects in various conditions. The result profile of Fig. 11 is also shown.

We calculated the temperature change at 0.3 mm from the skin surface, where thermoreceptors are said to exist.

In the calculation, we assumed the initial temperature of the contact object was set to 20, 25, and 30°C as shown in the figure, while the initial temperature of the skin was set to 33.6°C to match the initial temperature in Fig. 11. The thermal properties of the person were set to the value as the dermis in Table I. The parameters of other objects are shown in the table.

Note that the plots of Fig. 11 are the surface temperature not measured inside the skin. Therefore, they are not exactly equivalent comparisons. The temperature at 0.3 mm from the surface under ultrasound cooling is estimated to be 1.6 K above each plot at the maximum, assuming that the thermal conductivity of epidermis is 0.24 W/(m · K) and that the heat flux at the surface is -1.3×10^3 W/m². At the same time, considering the effect of blood flow, the theoretical value is revised upward. In addition, we assumed the uniform thermal conductivity of dermis that is higher than that of epidermis. When we consider the lower thermal conductivity near the skin surface, the theoretical values move upward more. More exact comparison needs precise model of the blood, which is left as the future work.

VII. DISCUSSION

In the results of Experiment 1, rapid cooling was seen when both the ultrasound and water mist were provided simultaneously. In a previous study using a contact-type Peltier device [13], a thermal sensation was displayed at a temperature change rate of -3.0 K/s. In a previous study [26], the steepest temperature drop of cold air transported by the ultrasound beam was -0.5 K/s. By contrast, the temperature change in the present study was -4.6 K/s at a minimum, suggesting that this is a faster phenomenon than the heat conduction into the cold air. Such rapid cooling is achieved by the vaporization heat of the water mist. In another previous study [29], the results of cooling using a Bessel beam and mist were

TABLE I
THERMAL PHYSICAL PROPERTIES

	Density [g/cm ³]	Specific heat [J/(g · K)]	Thermal conductivity [W/(m · K)]
Epidermis	1.20	3.59	0.24
Dermis	1.20	3.30	0.45
Iron	7.87	0.461	67.0
Acrylic	1.18	1.50	0.21
Paper	0.72	1.30	0.06
Natural rubber	0.16	1.88	0.134

reported. In that study, vaporization heat was used, but the temperature change rate was -1.3 K/s, which was slower than the current result. The possible factors that create the difference are the ultrasound energy density and the mist condition. In the former system, the mist flowed in the Bessel beam, where the liquid water was vaporized while vapor pressure increased during the transport.

During Experiment 2, the cooling effect decreased when the distance was longer than 50 cm under the current condition. The main reason is considered to be the decrease in the ultrasound power density.

At a distance of within 50 cm, the amount of mist supplied did not affect the cooling effect. By contrast, the cooling effect was influenced by the mist direction. One possible reason for this is the difference in the air flow around the skin. In the vertical mist-supply case shown in Fig. 3(i), the mist-air flow velocity becomes small (zero in the ideal case) on the skin surface as indicated by the fluid mechanics. As a result, the mist-air stays around the focal spot, which prevents heat removal and vaporization of the mist. By contrast, in a parallel supply case as shown in Fig. 3(iii), the mist-air is smoothly refreshed, increasing the efficiency of the cooling process. Another reason for the weakness of (i) is that the vapor pressure is already increased before the mist reached the skin surface since the mist was transported in the ultrasound beam.

In Experiment 3, the area cooled by mist vaporization was as small as 2 cm, and the temperature decreased by 3.3 K at 500 ms and 4.6 K in 1000 ms. The spatial resolution of the cooling sensation is known to be much lower than that of the vibrotactile and pressure sensations. In addition, the cooling response time is more than 500 ms [35] [36]. Thus, quick temperature drops with a smaller cold spot are sufficient for displaying various thermal sensations, such as material sensations with different thermal conductivities. This result showed that the setup can display the comparable temperature change when touching iron at room temperature in non-contact manner.

During Experiments 1–3, there are three data sets obtained under the similar conditions: the Focus+Mist condition shown in Fig. 5, case (i) in Fig. 7, and that shown in Fig. 11. There is a maximum difference of 2.1 K/s for these data. We consider the difference to be within the inevitable fluctuation of the system. Although the temperature and humidity slightly vary

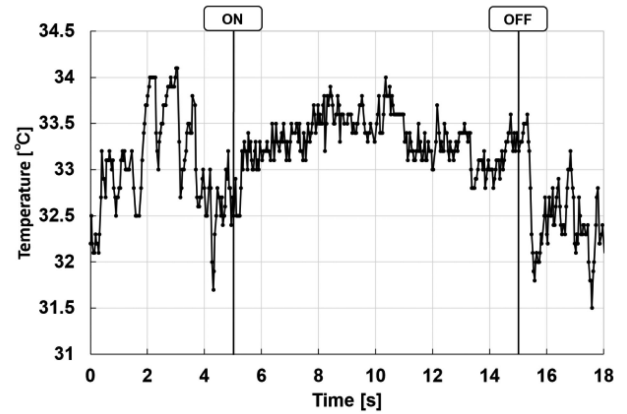


Fig. 18. Temperature change on the palm when the focused ultrasound is applied to the mist from the side.

within 1 K and 5%, respectively, this does not seem to cause such a difference in the cooling performance.

One concern regarding the temperature measurement is the influence of the mist image. A white water mist is visible, which can influence the temperature estimation of the palm surface when applying thermography. To confirm the measurement error, we measured the temperature of the palm surface with the mist flow in front of the palm surface while focused ultrasound was applied along the palm surface, where the ultrasound cooled the mist but did not irradiate the palm surface. That is, we created a situation in which a cooled mist was flowing in front of the palm, but the palm temperature was constant. Fig. 18 shows the temperature sequence under this situation as measured using thermography. In this case, the difference in temperature change was less than 1.5 K during irradiation. Similar measurements were conducted three times and they exhibited within ± 0.2 K. A temperature drop was not observed, which indicates that the image of the mist does not significantly affect the measurement.

As shown in Figs. 10 and 12, the size of the cold spot gradually increases. However, based on the authors' subjective report, the spatial spread of the cold sensation was not felt. In addition, with respect to the movement of cold spots on the palm, the authors clearly felt the motion of the cooling sensation. Clarifying the maximum perceivable speed of the cold spot will be an interesting item of future research.

The setup of this paper was performed by irradiating one focused ultrasound with four ultrasound phased arrays. Using the characteristics of the phased array, the rendering area can be magnified by enlarging the emission aperture. Multiple point cooling can be also achieved by using multi-focus rendering algorithms.

VIII. CONCLUSION

We proposed a method of remotely displaying cooling sensation, where the mist is instantly vaporized in a spot area near the user's skin by a focused ultrasound. We fabricated a prototype and examined its basic properties in producing a cooling sensation. First, we confirmed that the cooling effect occurs through a combination of the emission of a mist with

the irradiation of a focused ultrasound. Next, it was found that the cooling effect becomes saturated for an excessive amount of mist. We also found that the cooling performance depends on the distance between the device and target skin. Using a proper system setup as shown in Fig. 3(i), the temperature dropped by 4.6 K in 1 s and 3.3 K in the first 0.5 s on the skin surface immediately after irradiation. From the calculation of the heat flux, it was found that the system reproduces a comparable heat absorption to that of touching iron at room temperature. The diameter of the cold spot was approximately 2 cm, which was comparable to the ultrasound focus. In addition, we succeeded in creating a cooling spot moving on the skin surface in real time by continuously shifting the position of the focused ultrasound on a traveling path. Thus, we validated that a pinpoint remote cooling sensation can be displayed with our system. Owing to the pinpoint and fast temperature drop with low latency, it is expected that proposed method can be applied to real-time interaction systems. It is notable that the demonstrated cooling effect can coexist with a conventional ultrasound-driven vibrotactile stimulation.

In the future, our research will include an evaluation of the effect of the displayed cooling sensation on human bodies in terms of the psychophysical aspects. In addition, we will develop a multi-modal display system that combines the proposed remote cooling technique with the sensations of other sensory modalities. The mist used in the proposed system can potentially be utilized as a fog image display. Integrating all of these technical elements, we will continue our investigation on the appropriate design of thermal haptic feedback.

REFERENCES

- [1] T. Iwamoto, M. Tatezono, and H. Shinoda, "noncontact method for producing tactile sensation using airborne ultrasound," in *Proc. Eurohaptics*, 2008, pp. 504–513.
- [2] T. Hoshi, M. Takahashi, T. Iwamoto, and H. Shinoda, "Noncontact tactile display based on radiation pressure of airborne ultrasound," *IEEE Trans. Haptics*, vol. 3, no. 3, pp. 155–165, Jul./Sep. 2010.
- [3] G. Korres, and M. Eid, "Haptogram: Ultrasonic point-cloud tactile stimulation," *IEEE Access*, vol. 4, pp. 7758–7769, 2016.
- [4] I. Rakkolainen, E. Freeman, A. Sand, R. Raisamo, and S. Brewster, "A survey of mid-air ultrasound haptics and its applications," *IEEE Trans. Haptics*, vol. 14, no. 1, pp. 2–19, Jan./Mar. 2021.
- [5] T. Carter, S. A. Seah, B. Long, B. Drinkwater, and S. Subramanian, "UltraHaptics: Multi-point mid-air haptic feedback for touch surfaces," in *Proc. 26th ACM Symp. user interface Softw. Technol. (UIST '13)*, 2013, pp. 505–514.
- [6] R. Wettach, C. Behrens, A. Danielsson, and T. Ness, "A thermal information display for mobile application," in *Proc. MobileHCI '07*, 2007, pp. 182–185.
- [7] L. A. Jones, and H. Ho, "Warm or cool, large or small? The challenge of thermal displays," *IEEE Trans. Haptics*, vol. 1, no. 1, pp. 53–70, Jan./Jun. 2008.
- [8] L. A. Jones, "Perspectives evol. Tactile, hapticthermal displays," *Presence*, vol. 25, no. 3, pp. 247–252, 2016.
- [9] L. A. Jones, and M. Berris, "Material discrimination and thermal perception," 11th symposium on haptic interfaces for virtual environment and teleoperator systems, in *Proc. 11th Symp. Haptic Interfaces Virtual Environ. Teleoperator Syst., HAPTICS*, 2003, pp. 171–178.
- [10] H. N. Ho, and L. A. Jones, "Material identification using real and simulated thermal cues," in *Proc. 26th Annu. Int. Conf. IEEE Eng. Med. Biol. Soc.*, 2004, pp. 2462–2465.
- [11] H. N. Ho, and L. A. Jones, "Contribution of thermal cues to material discrimination and localization," *Percept. Psychophys.*, vol. 68, pp. 118–128, 2006.
- [12] A. Manasrah, N. Crane, R. Guldiken, and K. B. Reed, "Asymmetrically-applied hot and cold stimuli gives perception of constant heat," in *Proc. IEEE World Haptics Conf.*, 2017, pp. 484–489.
- [13] K. Sato, "Augmentation of thermal sensation on finger pad using stimuli for finger side," in *Proc. EuroHaptics*, 2016, Art. no. 371379.
- [14] K. Sato, and T. Maeno, "Presentation of rapid temperature change using spatially divided hot and cold stimuli," *J. Robot. Mechatronics*, vol. 25, no. 3, pp. 497–505, 2013.
- [15] G. Wilson, S. Brewster, M. Halvey, and S. Hughes, "Thermal icons: Evaluating structured thermal feedback for mobile interaction," in *Proc. 14th Int. Conf. Hum.-Comput. Interaction with Mobile Devices Serv.*, 2012, pp. 309–312.
- [16] D. G. Caldwell, S. Lawther, and A. Wardle, "Tactile percep. its application to des. Multi-modal cutan. Feedback syst.," in *Proc. Int. Conf. Robot. Automat.*, 1996.
- [17] M. Sakaguchi, K. Imai, and K. Hayakawa, "Development of high-speed thermal display using water flow," *Hum. Interface Manage. Inf. Inf. Knowl. Des. Eval., Lecture Notes Comput. Sci.*, vol. 8521, pp. 233–240, 2014.
- [18] K. Hayakawa, K. Imai, R. Honaga, and M. Sakaguchi, "High speed thermal display system that synchronized with the image using water flow," *Haptic Interaction*, vol. 277, pp. 69–74, 2015.
- [19] K. Hokoyama, Y. Kuroda, G. Kato, K. Kiyokawa, and H. Takemura, "Mugginess sensation: Exploring its principle and prototype design," in *Proc. IEEE World Haptics Conf.*, 2017, pp. 563–568.
- [20] S. Saga, "Thermal-radiation-based haptic display: Basic concept," in *Proc. IEEE World Haptics*, 2015, WIP-28 (Work-in-Progress Papers), pp. 2015–2006.
- [21] S. Saga, "Thermal-radiation-based haptic display - laser-emission-based radiation control," in *Proc. IEEE World Haptics*, 2019, WP2P.10 (Work-in-Progress Papers), pp. 2019–2007.
- [22] A. Sakai, T. Yamaguchi, H. Mitake, and S. Hasegawa, "Contactless warmth display using visible light LED for HMDVR," *TVRSJ*, vol. 24, no. 1, pp. 83–92, 2019. (In Japanese).
- [23] J.-H. Jun *et al.*, "Laser-induced thermoelastic effects can evoke tactile sensations," *Sci. Rep.*, vol. 5, 2015, Art. no. 11016.
- [24] R. A. Meyer, R. E. Walker, and V. B. Mountcastle, "A laser stimulator for the study of cutaneous thermal and pain sensations," *IEEE Trans. Biomed. Eng. BME*, vol. 23, no. 1, pp. 54–60, Jan. 1976.
- [25] J. Xu, Y. Kuroda, S. Yoshimoto, and O. Oshiro, "Non-contact cold thermal display by controlling low-temperature air flow generated with vortex tube," in *Proc. IEEE World Haptics Conf.*, 2019.
- [26] M. Nakajima, K. Hasegawa, Y. Makino, and H. Shinoda, "Remotely displaying cooling sensation via ultrasound-driven air flow," in *Proc. IEEE Haptics Symp.*, 2018, pp. 340–343.
- [27] K. Hasegawa, L. Qiu, A. Noda, S. Inoue, and H. Shinoda, "Electronically steerable ultrasound-driven long narrow air stream," *Appl. Phys. Lett.*, vol. 111, no. 6, 2017, Art. no. 064104.
- [28] M. Nakajima, K. Hasegawa, Y. Makino, and H. Shinoda, "Remotely displaying cooling sensation using ultrasound mist beam," in *Proc. Asia Haptics, Incheon, Korea: Live Demo Presentation*, 2018.
- [29] M. Nakajima, Y. Makino, and H. Shinoda, "Remote cooling sensation presentation controlling mist in midair," in *Proc. IEEE/SICE Int. Symp. System Integration*, 2020, pp. 1238–1241.
- [30] M. A. Norasikin, D. M. Plasencia, G. Memoli, and S. Subramanian, "Sonic spray: A technique to reconfigure permeable mid-air displays," in *Proc. ACM Int. Conf. Interactive Surfaces Spaces (ISS'19)*, 2019 pp. 113–122.
- [31] M. A. Norasikin, D. M. Plasencia, S. Polychronopoulos, G. Memoli, Y. Tokuda, and S. Subramanian, "SoundBender: Dynamic acoustic control behind obstacles," in *Proc. 31st Annu. ACM Symp. user interface Softw. Technol. (UIST'18)*, pp. 247–259, doi: <https://doi.org/10.1145/3242587.3242590>.
- [32] S. Inoue, Y. Makino, and H. Shinoda, "Scalable architecture for airborne ultrasound tactile display," in *Proc. International AsiaHaptics Conf. AsiaHaptics*, 2016.
- [33] S. Suzuki, S. Inoue, M. Fujiwara, Y. Makino, and H. Shinoda, "AUTD3: Scalable airborne ultrasound tactile display," *IEEE Trans. Haptics*, to be published, doi: [10.1109/TOH.2021.3069976](https://doi.org/10.1109/TOH.2021.3069976).
- [34] A. Dufour *et al.*, "Thermal sensitivity in humans at the depth of thermal receptor endings beneath the skin: Validation of a heat transfer model of the skin using high-temporal resolution stimuli," *Eur J Appl Physiol*, vol. 120, pp. 1509–1518, 2020. [Online]. Available: <https://doi.org/10.1007/s00421-020-04372-y>
- [35] H. Fruhstorfer, H. Guth, and U. Pfaff, "Thermal reaction time as a function of stimulation site," *Pflugers Arch*, vol. 335, pp. R49, 1972.

- [36] C. J. Fowler, K. Sitzoglou, Z. Ali, and P. Halonen, "The conduction velocities of peripheral nerve fibres conveying sensations of warming and cooling," *J. Neurol., Neurosurgery Psychiatry*, vol. 51, no. 9, pp. 1164–1170, 1988.



Mitsuru Nakajima (Member, IEEE) received the M.S. degree in 2018 from the Department of Complexity Science and Engineering, University of Tokyo, Chiba, Japan, where he has been working toward the Ph.D. degree with the Graduate School of Frontier Sciences, since 2018. His research interests include haptics, focusing on ultrasound haptics, and thermal sensation.



Keisuke Hasegawa (Member, IEEE) received the B.E. degree in information physics and the M.E. and Ph.D. degrees in information science and technology from the University of Tokyo, Tokyo, Japan, in 2009, 2011, and 2014, respectively. Since 2020, he has been an Assistant Professor (Lecturer) with the Graduate School of Information Science and Technology, University of Tokyo. He was a Postdoc Research Fellow and a Research Associate with the University of Tokyo. His current research interests include haptic technologies, applied physics, and human-oriented informatics.



Yasutoshi Makino received the Ph.D. degree in information science and technology from the University of Tokyo, Tokyo, Japan, in 2007. He is currently an Associate Professor with the Department of Complexity Science and Engineering, University of Tokyo. He was a Researcher for two years with the University of Tokyo and an Assistant Professor with Keio University, Tokyo, Japan, from 2009 to 2013. From 2013, he moved to the University of Tokyo as a lecture, and since 2017, he has been an Associate Professor. His research focuses on haptic interactive systems.



Hiroyuki Shinoda (Member, IEEE) received the B.S. degree in applied physics, the M.S. degree in information physics, and the Ph.D. degree in engineering from the University of Tokyo, Tokyo, Japan, in 1988, 1990, and 1995, respectively. He is currently a Professor with the Graduate School of Frontier Sciences, University of Tokyo. From 1995 to 1999, he was an Associate Professor with the Department of Electrical and Electronic Engineering, Tokyo University of Agriculture and Technology, Fuchu, Japan. After a period with UC Berkeley, as a Visiting Scholar in 1999, he was an Associate Professor with the University of Tokyo from 2000 to 2012. His research interests include information physics, haptics, mid-air haptics, two-dimensional communication, and application systems related to them. He is a Member of SICE, IEEJ, RSJ, JSME, VRSJ, and ACM.